Interfacial Shear Viscosity at Fluid-Fluid Interfaces

D. T. WASAN, LALIT GUPTA, and M. K. VORA

Illinois Institute of Technology, Chicago, Illinois 60616

Fluid-fluid interfaces containing surface-active agents or macromolecules exhibit interfacial shear viscosity phenomena. The purpose of this paper is to investigate theoretically the dynamics of liquid-liquid and liquid-gas interfaces containing surfactants, and to establish the validity of the proposed model from shear flow data at uncontaminated interfaces.

A theoretical analysis for the measurement of interfacial shear viscosity at liquid-liquid interfaces with an improved viscous traction surface viscometer is presented. The analysis takes into account the finite depths of the two liquids and permits interpretation of the experimental results in terms of interfacial shear viscosities at the liquid-gas interface in addition to the liquid-liquid interface. Results of the present analysis clearly show a strong coupling of interfacial and bulk fluid flows.

Extensive measurements of the interfacial velocities at a xylene-water interface were made. A cetane-water interface was also studied. Interfacial flow data for uncontaminated systems were found to be in excellent agreement with theory.

The flow behavior at fluid-fluid interfaces depends on the purity of the interface. It is well known that surface-active agents and other impurities present in either the drop phase or the continuous phase in a liquid-liquid system alter the flow and the shape of the drops (*18, 19, 21*). More recently, photographic observations of the passage of a liquid drop through a liquid-liquid interface in three-phase liquid-liquid systems revealed rather peculiar hydrodynamic behavior at an impure interface when compared to that at a pure interface (*27*). The hydrodynamics of coalescence of liquid drops in emulsions is known to differ in systems with and without surfactants (*11*). The reduction in mass transfer rates due to the presence of surfactants and other impurities at fluid-fluid interfaces has been reported by many investigators (*7, 12, 18, 21*).

Willard Gibbs (*9*) in 1878 showed theoretically that surfactants or impurities, especially if the impurity is a high molecular weight analog of the surfactant, adsorb at interfaces. The presence of these macromolecules or contaminants at interfaces results not only in a lowering of the interfacial tension but also in additional, intrinsic, hydrodynamic resistance to flow of which interfacial shear viscosity is a measure.

The interface between two pure liquids or between a pure liquid and its vapor or a gas exhibits no viscosity other than bulk viscosity. However, solutions of macromolecules or surface-active agents are characterized by interfacial shear viscosity which is defined as the ratio between the shear stress and the shear rate in the plane of the interface. The role of this increased resistance to tangential shear resulting from the segregation of surface-active agents in the interfacial layers has been recognized in a few specific instances, such as in Marangoni instability (*29*), suspension polymerization (*16*), and emulsion stability (*15*). However its importance in many transport processes has been generally ignored, probably because the solution of the hydrodynamic equations of motion in the neighborhood of viscous fluid-fluid interfaces is not available to calculate interfacial shear viscosities from earlier experimental data.

The earlier observations of interfacial shear viscosity were qualitative in nature and were concerned with monomolecular films, insoluble monolayers, and surface-active agents at gas-liquid interfaces (*8, 14* to *16*). The interfacial shear viscosity at liquid-liquid interfaces has received scant attention (*24*). Cumper and Alexander (*4*) measured the interfacial viscosity of spread protein monolayers and adsorbed films at an oil-water interface by oscillating a platinum needle attached to a heavy metal bob at the interface. Sherman (*28*) investigated the influence of increasing concentration of the nonionic emulsifier sorbitan sesquioleate and the effect of aging on the interfacial viscosity at the mineral oil-distilled water interface using the oscillating disk method. The same technique was used by Blakey and Lawrence (*1*) to measure the interfacial viscosity of soap solutions and by Criddle and Meader (*3*) to investigate the effects of some surfactants on the interfacial viscosity at oil-water interfaces. Davies and Mayers (*5*) developed a circular "viscous traction" viscometer to determine the interfacial viscosities of various monolayers at the benzene-water and ethyl acetate-water interfaces. Recently, Karam et al. (*17*) used a rotational torsion surface viscometer to obtain rheological data for polymeric surfactants at liquid-liquid interfaces.

The techniques used by these investigators suffer from various shortcomings. The most basic of these is the fact that most of these methods do not involve a simple geometry, and as a result the velocity at a fluid-fluid interface cannot be obtained analytically. Consequently, the actual values for the interfacial shear viscosity are highly uncertain (*24*). Furthermore, the lack of mathematical analysis makes it difficult to obtain the exact shear rate at which the interfacial viscometric measurement is made. These shortcomings are eliminated in the improved viscous-traction interfacial viscometer developed by Burton and Mannheimer (*2*) and later used by Israel (*13*), Pintar (*25, 26*), Mannheimer (*22*), Vora (*30*), and Mannheimer and Schechter (*23*). The instrument is described later in the paper.

It is the purpose of this paper to investigate theoretically the dynamics of liquid-liquid and liquid-gas interfaces containing surfactants. The hydrodynamic equations of motion are solved to yield the steady state velocity distributions at the fluid-fluid interfaces under the assumption of

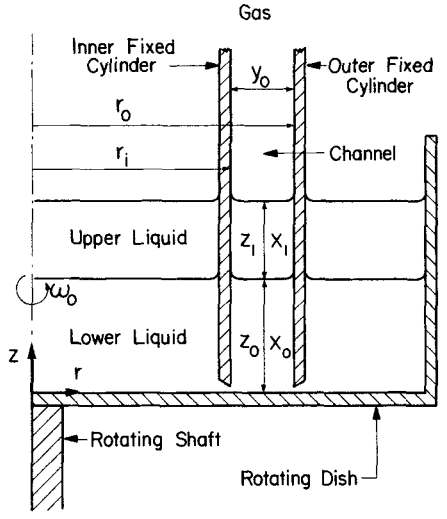

Fig. 1. Schematic diagram of the viscous traction surface viscometer.

laminar flow resulting from slow rotation of the dish containing the liquids. We shall see that our analysis permits interpretation of the experimental results in terms of the interfacial shear viscosity at the liquid-liquid as well as the liquid-gas interfaces. The validity of the proposed model will be established from shear flow data at uncontaminated interfaces.

THEORETICAL ANALYSIS

The specific geometry which we wish to consider is sketched in Figure 1. The viscometer consists of a flat-bottomed dish containing the fluids and two stationary, concentric cylinders. The cylinders are held vertically and so placed that they almost touch the bottom of the dish. The dish is rotated, causing the fluids in the channel between the cylinders to rotate, and the stationary channel walls tend to shear the fluids. This enhances the effect of the interface and makes it possible to use this method to determine interfacial viscosity.

The mathematical model to be used here assumes that the circular channel can be approximated by an infinitely long rectilinear channel. This assumption has been shown to be valid as long as the channel width (y_0) is small compared to the radius of the outer stationary cylinder (23, 25). It will also be assumed that there is no gap between the channel walls and the rotating dish. This assumption has been found to be valid even though a small gap is actually present (25). The fluids in the channel will be assumed to be Newtonian and incompressible. The bulk viscosity of the gas, air in most cases, will be considered negligible with respect to the bulk viscosities of the liquids. The flow in the channel will be assumed to be steady and laminar. The interfaces, liquid-liquid as well as liquid-gas, shall be considered flat for the purpose of simplicity and assumed to exhibit Newtonian interfacial shear viscosities, that is, the viscosity is not a function of the interfacial shear rate.

With the above assumptions, and placing the origin of coordinates at the floor and one of the channel walls with the x axis taken along the channel wall and the y axis along the floor, we can give the velocities $\hat{V}$ and V in the channel by the following boundary value problem:

$$\frac{\partial^2 \hat{V}}{\partial x^2} + \frac{\partial^2 \hat{V}}{\partial y^2} = 0, \quad 0 \leq x \leq x_0 \tag{1}$$

$$\frac{\partial^2 V}{\partial x^2} + \frac{\partial^2 V}{\partial y^2} = 0, \quad x_0 \leq x \leq x_0 + x_1 \tag{2}$$

The boundary conditions are

$$\hat{V}(x, 0) = 0 \qquad 0 \leq x \leq x_0 \tag{3}$$

$$\hat{V}(x, y_0) = 0 \qquad 0 \leq x \leq x_0 \tag{4}$$

$$\hat{V}(0, y) = (r_i + y)\omega_0 \qquad 0 \leq y \leq y_0 \tag{5}$$

$$\hat{\eta} \frac{\partial \hat{V}}{\partial x}(x_0, y) - \eta \frac{\partial V}{\partial x}(x_0, y) = \hat{\epsilon} \frac{\partial^2 \hat{V}}{\partial y^2}(x_0, y) \qquad 0 \leq y \leq y_0 \tag{6}$$

$$V(x, 0) = 0, \qquad x_0 \leq x \leq x_0 + x_1 \tag{7}$$

$$V(x, y_0) = 0, \qquad x_0 \leq x \leq x_0 + x_1 \tag{8}$$

$$\hat{V}(x_0, y) = V(x_0, y), \quad 0 \leq y \leq y_0 \tag{9}$$

$$\eta \frac{\partial V}{\partial x}(x_0 + x_1, y) = \epsilon \frac{\partial^2 V}{\partial y^2}(x_0 + x_1, y), \quad 0 \leq y \leq y_0 \tag{10}$$

Equations (6) and (10) result from momentum balances at the liquid-liquid and liquid-gas interfaces, respectively, under the assumptions of negligible mass of the interfaces and negligible mass transfer across the interfaces.

The general solution for Laplace's Equations (1) and (2) is given by

$$\hat{V} = \sum_{n=1}^{\infty} [\hat{a}_n \cosh \hat{\lambda}_n x \sin \hat{\lambda}_n y + \hat{b}_n \sinh \hat{\lambda}_n x \sin \hat{\lambda}_n y + \hat{c}_n \cosh \hat{\lambda}_n x \cos \hat{\lambda}_n y + \hat{d}_n \sinh \hat{\lambda}_n x \cos \hat{\lambda}_n y] \tag{11}$$

$$V = \sum_{n=1}^{\infty} [a_n \cosh \lambda_n x \sin \lambda_n y + b_n \sinh \lambda_n x \sin \lambda_n y + c_n \cosh \lambda_n x \cos \lambda_n y + d_n \sinh \lambda_n x \cos \lambda_n y] \tag{12}$$

where $\hat{a}_n$, $\hat{b}_n$, $\hat{c}_n$, $\hat{d}_n$, $\hat{\lambda}_n$, a_n, b_n, c_n, d_n, and λ_n are constants to be evaluated from the boundary conditions.

Equation (3) requires that $\hat{c}_n = \hat{d}_n = 0$. From Equation (4) it follows that $\hat{\lambda}_n = n\pi/y_0$. Equations (7) and (8) require that $c_n = d_n = 0$ and $\lambda_n = n\pi/y_0$, respectively. Application of the boundary condition at the floor [Equation (5)] yields

$$\sum_{n=1}^{\infty} \hat{a}_n \sin(n\pi y/y_0) = (r_i + y)\,\omega_0 \tag{13}$$

The constant $\hat{a}_n$ evaluated using the principle of orthogonality

$$\int_0^{y_0} \sin(n\pi y/y_0) \sin(m\pi y/y_0) dy = y_0/2, \quad m = n = 0, \quad m \neq n \tag{14}$$

is given by

$$\hat{a}_n = 4\omega_0 (r_i + y_0/2)/n\pi = 4\bar{V}_b/n\pi, \quad n \text{ odd}$$
$$= -2\omega_0 y_0/n\pi \quad , \quad n \text{ even} \tag{15}$$

Applying the boundary conditions given by Equations (6), (9), and (10), we have

$$-[\hat{\eta}\cosh n\pi D + (\hat{\epsilon}\, n\pi/y_0)\sinh n\pi D]\,\hat{b}_n + [\eta \sinh n\pi D]\,a_n + [\eta\cosh n\pi D]\,b_n = [\hat{\eta}\sinh n\pi D + (\hat{\epsilon}\, n\pi/y_0)\cosh n\pi D]\,\hat{a}_n \tag{16}$$

$$-[\sinh n\pi D]\,\hat{b}_n + [\cosh n\pi D]\,a_n + [\sinh n\pi D]\,b_n = [\cosh n\pi D]\,\hat{a}_n \tag{17}$$

$$[\eta \sinh n\pi(D + D_1) + (\epsilon\, n\pi/y_0)\cosh n\pi(D + D_1)]\,a_n + [\eta\cosh n\pi(D + D_1) + (\epsilon\, n\pi/y_0)\sinh n\pi(D + D_1)]\,b_n = 0 \tag{18}$$

Here $D = x_0/y_0$ and $D_1 = x_1/y_0$.

Simultaneously solving Equations (16), (17), and (18) for $\hat{b}_n$, a_n, and b_n, we get

$$\hat{b}_n = -\hat{a}_n\{[\hat{\eta}\sinh n\pi D + (\hat{\epsilon}\, n\pi/y_0)\cosh n\pi D][\eta\cosh n\pi D_1 + (\epsilon\, n\pi/y_0)\sinh n\pi D_1] + [\eta\cosh n\pi D][\eta\sinh n\pi D_1 + (\epsilon\, n\pi/y_0)\cosh n\pi D_1]\}/E_n \tag{19}$$

$$a_n = \hat{a}_n\hat{\eta}[\eta\cosh n\pi(D + D_1) + (\epsilon\, n\pi/y_0)\sinh n\pi(D + D_1)]/E_n \tag{20}$$

$$b_n = -\hat{a}_n\hat{\eta}[\eta\sinh n\pi(D + D_1) + (\epsilon\, n\pi/y_0)\cosh n\pi(D + D_1)]/E_n \tag{21}$$

where

$$\left.\begin{aligned} E_n = {} & [\hat{\eta}\cosh n\pi D + (\hat{\epsilon}\, n\pi/y_0)\sinh n\pi D] \\ & [\eta\cosh n\pi D_1 + (\epsilon\, n\pi/y_0)\sinh n\pi D_1] \\ & + [\eta\sinh n\pi D][\eta\sinh n\pi D_1 \\ & + (\epsilon\, n\pi/y_0)\cosh n\pi D_1] \end{aligned}\right\} \tag{22}$$

Hence

$$\left.\begin{aligned} \hat{V} = {} & \sum_{n=1}^{\infty}\hat{a}_n \sin(n\pi y/y_0) \\ & \{\hat{\eta}[\eta\cosh n\pi D_1 + (\epsilon\, n\pi/y_0)\sinh n\pi D_1] \\ & \cosh[n\pi(x - x_0)/y_0] - \eta[\eta\sinh n\pi D_1 \\ & + (\epsilon\, n\pi/y_0)\cosh n\pi D_1]\sinh[n\pi(x - x_0)/y_0] \\ & - (\hat{\epsilon}\, n\pi/y_0)[\eta\cosh n\pi D_1 + (\epsilon\, n\pi/y_0) \\ & \sinh n\pi D_1]\sinh[n\pi(x - x_0)/y_0]\}/ \\ & \{[\hat{\eta}\cosh n\pi D + (\hat{\epsilon}\, n\pi/y_0)\sinh n\pi D] \\ & [\eta\cosh n\pi D_1 + (\epsilon\, n\pi/y_0)\sinh n\pi D_1] \\ & + [\eta\sinh n\pi D][\eta\sinh n\pi D_1 \\ & + (\epsilon\, n\pi/y_0)\cosh n\pi D_1]\} \end{aligned}\right\} \tag{23}$$

$$\left.\begin{aligned} V = {} & \sum_{n=1}^{\infty}\hat{a}_n \sin(n\pi y/y_0)\,\hat{\eta} \\ & \{\eta\cosh[n\pi(x - x_0 - x_1)/y_0] \\ & - (\epsilon\, n\pi/y_0)\sinh[n\pi(x - x_0 - x_1)/y_0]\}/ \\ & \{[\hat{\eta}\cosh n\pi D + (\hat{\epsilon}\, n\pi/y_0)\sinh n\pi D] \\ & [\eta\cosh n\pi D_1 + (\epsilon\, n\pi/y_0)\sinh n\pi D_1] \\ & + [\eta\sinh n\pi D][\eta\sinh n\pi D_1 \\ & + (\epsilon\, n\pi/y_0)\cosh n\pi D_1]\} \end{aligned}\right\} \tag{24}$$

Along the center line of the liquid-liquid interface, $x = x_0$, $y = y_0/2$, and $\hat{V} = \hat{V}_c$. Also, for deep channels, that is, $D > 2/\pi$, only the first term in the series on the right-hand side of Equation (23) needs to be considered, and $\sinh n\pi D \doteq \cosh n\pi D$. Then

$$\hat{V}_c = \frac{(4\bar{V}_b/\pi\cosh\pi D)\,\hat{\eta}}{(\hat{\eta} + \hat{\epsilon}\,\pi/y_0) + \eta\dfrac{\eta\sinh\pi D_1 + (\epsilon\,\pi/y_0)\cosh\pi D_1}{\eta\cosh\pi D_1 + (\epsilon\,\pi/y_0)\sinh\pi D_1}} \tag{25}$$

Along the center line of the liquid-gas interface, $x = x_0 + x_1$, $y = y_0/2$, and $V = V_c$. For a deep channel, V_c is given by

$$V_c = \frac{(4\bar{V}_b/\pi\cosh\pi D)\,\hat{\eta}\,\eta/[\eta\cosh\pi D_1 + (\epsilon\,\pi/y_0)\sinh\pi D_1]}{(\hat{\eta} + \hat{\epsilon}\,\pi/y_0) + \eta\dfrac{\eta\sinh\pi D_1 + (\epsilon\,\pi/y_0)\cosh\pi D_1}{\eta\cosh\pi D_1 + (\epsilon\,\pi/y_0)\sinh\pi D_1}} \tag{26}$$

From Equations (25) and (26) we have

$$\hat{V}_c/V_c = [\eta\cosh\pi D_1 + (\epsilon\,\pi/y_0)\sinh\pi D_1]/\eta \tag{27a}$$

or

$$\frac{\epsilon\pi}{\eta y_0} = \frac{(\hat{V}_c/V_c - \cosh\pi D_1)}{\sinh\pi D_1} \tag{27b}$$

For uncontaminated systems, $\hat{\epsilon} = \epsilon = 0$. Then the interfacial center-line velocities reduce to

$$\hat{V}_c^* = \frac{(4\bar{V}_b/\pi\cosh\pi D)\,\hat{\eta}}{\hat{\eta} + \eta\tanh\pi D_1} \tag{28}$$

and

$$V_c^* = \frac{(4\bar{V}_b/\pi\cosh\pi D)\,\hat{\eta}}{\cosh\pi D_1\,(\hat{\eta} + \eta\tanh\pi D_1)} \tag{29}$$

where the asterisk denotes that $\hat{\bullet} = \epsilon = 0$.

From Equations (28) and (29) we get

$$\hat{V}_c^*/V_c^* = \cosh\pi D_1 \tag{30}$$

Equations (25) and (28) yield

$$\hat{V}_c^*/\hat{V}_c = \frac{(\hat{\eta} + \hat{\epsilon}\,\pi/y_0) + \eta\dfrac{\eta\sinh\pi D_1 + (\epsilon\,\pi/y_0)\cosh\pi D_1}{\eta\cosh\pi D_1 + (\epsilon\,\pi/y_0)\sinh\pi D_1}}{\hat{\eta} + \eta\tanh\pi D_1}$$

or

$$\frac{\hat{\epsilon}\pi}{(\hat{\eta}+\eta)y_0} = \frac{\hat{\eta}}{\hat{\eta}+\eta}\left(\frac{\hat{V}_c^*}{\hat{V}_c} - 1\right) + \frac{\eta}{\hat{\eta}+\eta}\left\{\frac{\hat{V}_c^*}{V_c}\tanh \pi D_1 - \frac{\eta \sinh \pi D_1 + (\epsilon\pi/y_0)\cosh \pi D_1}{\eta \cosh \pi D_1 + (\epsilon\pi/y_0)\sinh \pi D_1}\right\} \quad (31)$$

Equations (27) and (31) relate ϵ and $\hat{\epsilon}$ to the bulk viscosities (η and $\hat{\eta}$) of the two liquids, the geometry of the viscometer (y_0, x_0, and x_1), and experimentally determined interfacial velocities ($\hat{V}_c^*$, $\hat{V}_c$, and V_c). When D_1 is large enough to justify $\sinh \pi D_1 \doteq \cosh \pi D_1$, Equations (27) and (31) reduce to

$$\frac{\epsilon\pi}{\eta y_0} = \frac{(\hat{V}_c/V_c)}{\sinh \pi D_1} - 1 \quad (32)$$

$$\frac{\hat{\epsilon}\pi}{(\hat{\eta}+\eta)y_0} = \frac{\hat{V}_c^* - \hat{V}_c}{\hat{V}_c} \quad (33)$$

Now if the interfacial viscosities ϵ and $\hat{\epsilon}$ are Newtonian and hence independent of shear rate, then for a particular D_1 for a specific system (with fixed η and $\hat{\eta}$), Equation (25) gives

$$\frac{\hat{V}_c}{\overline{V}_b} \propto \frac{1}{\cosh \pi D} \quad (34)$$

Furthermore, for deep channels with $D > 2/\pi$, we may approximate $\cosh \pi D$ by $e^{\pi D}/2$. A semilog plot of $\hat{V}_c/\overline{V}_b$ versus D will then be a straight line with a slope of $-\pi$. This straight line will be parallel to the one representing a system with negligible interfacial viscosities. It is thus possible to judge the Newtonian or non-Newtonian behavior of interfacial viscosities from such a semilog plot.

Analysis for a Curved Interface

As mentioned earlier, one of the assumptions of the model presented here is that the fluid-fluid interfaces in the channel are flat. The effect of this assumption on the interfacial center-line velocity has been investigated for liquids or solutions with negligible surface shear viscosity (*10*). Furthermore, we have also developed a theory which takes into account the effect of the curved interface on both the Newtonian and the non-Newtonian characteristics of surface shear viscosity at gas-liquid interfaces; this is being presented elsewhere (*26, 31*). However, as yet there is no theory for the effect of curved interfaces on interfacial viscosity measurements at liquid-liquid interfaces.

EXPERIMENTAL MEASUREMENTS WITH AN IMPROVED VISCOUS TRACTION SURFACE VISCOMETER

The aim of the experimental program was to test the validity of the model presented for uncontaminated systems exhibiting negligible interfacial viscosity.

A sectional view of the apparatus used is shown in Figure 2. A brass dish (*A*) is attached to a central rotating shaft (*B*). Two concentric brass cylinders (*C*, *D*) glued at the top to a plexiglass holder (*E*) form the 3/8-in. wide channel. The holder is supported by three bolts (*F*) which form the frame of the instrument. Concentricity of the cylinders with respect to the shaft is ensured with the help of a centering rod (*G*) capable of insertion into the shaft. The motive power is provided by a 0.1-hp., variable-speed universal electric motor (*M*) which is connected to the shaft through a 15:1 worm gear (*I*). Liquid depths at the center of the channel are measured with a stainless steel probe (*J*). The probe has a tapered tip and a small flange (*K*) and can be inserted through any of the three holes (*L*) in the holder. The interface is observed through a hole (*N*) in the holder.

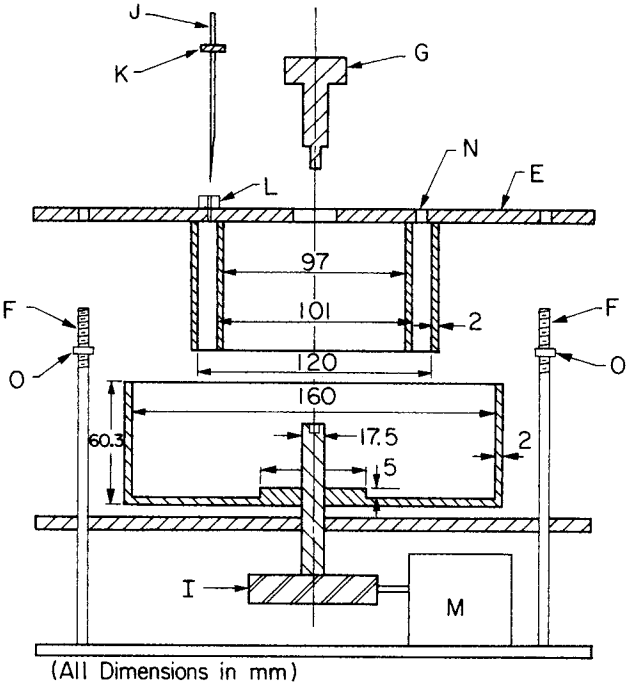

Fig. 2. Cross section of the surface viscometer (symbols as explained in the text).

The experimental procedure is as follows:

A calculated amount of the heavier liquid was poured into the dish. After positioning and leveling the plexiglass holder, it was adjusted with the help of nuts (*O*) so that the gap between the lower tip of the concentric cylinders and the floor of the dish was 1/64 in. as determined from cathetometer readings on the flange (*K*). The concentric cylinders were centered by placing the centering rod in position. The interface in the channel was illuminated with a light source above the instrument.

The depth of the heavier liquid (deionized water) was obtained from cathetometer readings on the flange taken for two positions of the probe: one when the tip of the probe just penetrated the surface and the other when it made contact with the floor of the dish. Calculated amounts of the lighter liquid (a reagent grade xylene) were separately introduced into the channel, the central portion, and the annulus between the outer cylinder and the wall of the dish to yield the same height in the three sections. The depth of the lighter liquid was then determined from a cathetometer reading on the flange when the probe just penetrated the upper interface. A Teflon particle (diameter $\doteq$ 0.02 cm.) was then dropped through the viewing hole so that it floated at the center line of the channel. It was lowered to the liquid-liquid interface from the liquid-gas interface with a thin aluminum wire. This procedure was necessitated by the frequent migration of the particle from the liquid-liquid to the liquid-gas interface when it was introduced prior to the lighter liquid. The electric motor was turned on and the powerstat adjusted to obtain the desired speed of rotation of the dish. The time taken by the particle to complete one revolution was measured with a stop watch.

Theoretically [from Equations (25) and (26) for deep channels], if the particle is off-center by $\pm$ 5% of the center-line distance ($y_0/2$) from the wall, an error of only 0.4% in

the measurement of velocity will result; for ± 10% deviation from the center line, the error will be 1.5% and for ± 15%, it will be 3.4%. Lining up the particle with the naked eye, with reference to an appropriately inscribed circle at the base of the channel, will not, in any case, result in a deviation of more than ± 10% and hence the error so incurred will always be less than 1.5%.

Determination of Curvature Effects

It was necessary to determine the shape of the curved interfaces in order to assess their effect on the interfacial centerline velocity. Theoretically, the interfacial profile (*10, 20*) between two fluids can be shown to depend on the density difference between the fluids, the interfacial tension, and the contact angle. For the systems under consideration in the present work, density measurements were made with the help of a specific gravity bottle. A Cence-Du Nouy Interfacial Tensiometer (No. 70545) was used to determine the interfacial tension. Bulk viscosity measurements were made with a Brookfield Synchrolectric Viscometer. The contact angle for liquid-air interfaces was determined by the tilting plate method described by Davies and Rideal (*6*). In view of the considerable difference between advancing and receding contact angles for liquid-liquid interfaces (*6*), the tilting plate method was not used to determine the contact angle for such systems. Instead, the interfacial profile between two plates 3/8 in. apart was determined and plotted. The contact angle was calculated from the slope of the curve at either wall.

RESULTS AND DISCUSSION

Theoretical Results

For deep channels, that is, $D > 2/\pi$, we may consider only the first term in the series expression for the velocity given by Equation (23) and approximate $\sinh \pi D$ and $\cosh \pi D$ by $e^{\pi D}/2$ without incurring an error of more than 2%. At the liquid-liquid interface, $x = x_0$, we can write the interfacial velocity equation in the following form:

$$\hat{V} = \frac{8\bar{V}_b}{\pi e^{\pi D}} \frac{\sin(\pi y/y_0)}{1 + \frac{\pi\epsilon}{\hat{\eta} y_0} + \frac{\eta}{\hat{\eta}} \left\{ \frac{\tanh \pi D_1 + \frac{\epsilon\pi}{\eta y_0}}{1 + \frac{\epsilon\pi}{\eta y_0} \tanh \pi D_1} \right\}} \tag{35}$$

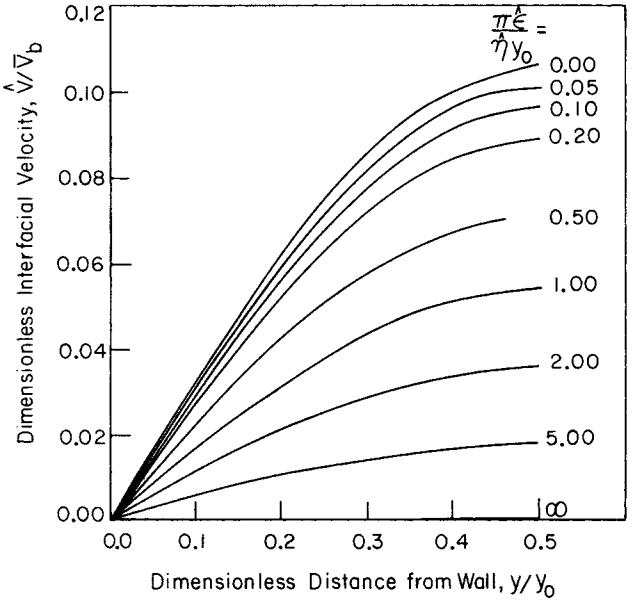

Fig. 3. Theoretical interfacial velocity profiles for $x_0/y_0 = 1.0$; $x_1/y_0 = 0.01$; $\eta/\hat{\eta} = 1$; $\pi\epsilon/\eta y_0 = 0$.

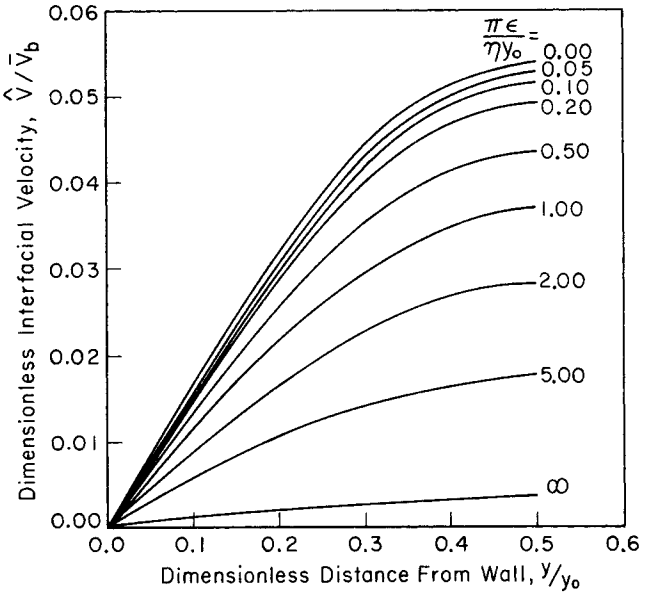

Fig. 4. Theoretical interfacial velocity profiles for $x_0/y_0 = 1.0$; $x_1/y_0 = 0.1$; $\eta/\hat{\eta} = 1$; $\hat{\pi\epsilon}/\eta y_0 = 1$.

Figure 3 depicts the effect of the dimensionless interfacial viscosity $(\hat{\pi\epsilon}/\hat{\eta} y_0)$ on the velocity profile at the liquid-liquid interface when all other parameters are held constant. An increase of $(\hat{\pi\epsilon}/\hat{\eta} y_0)$ results in decreased velocities at any given distance from the wall. Figure 4 reveals the considerable lowering of the interfacial velocity $\hat{V}/\bar{V}_b$ due to increasing relative interfacial viscosity $(\pi\epsilon/\eta y_0)$ at the liquid-gas interface. This effect is more pronounced at the low value of upper liquid depth (D_1) considered here. For deep channels, that is, for values of $D_1 = x_1/y_0 > 2/\pi$, $\tanh \pi D_1 \doteq 1$ and the group $(\tanh \pi D_1 + \epsilon\pi/\eta y_0)/(1 + \tanh \pi D_1\, \epsilon\pi/\eta y_0)$ in Equation (35) tends to unity irrespective of the value of $(\pi\epsilon/\eta y_0)$. The velocity $(\hat{V}/\bar{V}_b)$ at the liquid-liquid interface then becomes independent of the relative interfacial viscosity $(\pi\epsilon/\eta y_0)$ at the liquid-gas interface.

Figures 5 and 6 depict the effects of the ratio of the bulk viscosities $(\eta/\hat{\eta})$, the relative interfacial viscosities $(\hat{\pi\epsilon}/\hat{\eta} y_0$ and $\pi\epsilon/\eta y_0)$, and the dimensionless depths of the two liquids $(x_0/y_0$ and $x_1/y_0)$ on the interfacial midchannel velocity. Figure 5 shows that increasing $(\eta/\hat{\eta})$ or increasing $(\hat{\pi\epsilon}/\hat{\eta} y_0)$ serves to lower the interfacial velocity at a given value of $(\pi\epsilon/\eta y_0)$. Increasing depths of the liquids have the same effect on the interfacial velocity. The effect of increasing x_1/y_0, however, is manifested only for $x_1/y_0 < 2/\pi$ as seen earlier.

An interesting observation can be made from Figure 6. For $\pi\epsilon/\eta y_0 = 0$, increasing the dimensionless upper depth (x_1/y_0) results in decreased velocities, whereas for $(\pi\epsilon/\eta y_0) = 2$, increasing the upper depth (x_1/y_0) results in increased velocities, everything else being held constant. In fact, the former trend exists for $(\pi\epsilon/\eta y_0) < 1$ and the latter for $(\pi\epsilon/\eta y_0) > 1$. For $(\pi\epsilon/\eta y_0) = 1$, the upper depth has no effect on the interfacial velocity at the liquid-liquid interfaces. This apparently anomalous behavior results from the interaction between the parameters $(\pi\epsilon/\eta y_0)$ and (x_1/y_0) in Equation (35). The above discussion is valid for the interfacial velocity at any distance

from the wall since it is related to the midchannel velocity by $\hat{V} = \hat{V}_c \sin(\pi y/y_0)$ as is readily seen from Equation (35).

The above discussion pertains to the velocity ($\hat{V}$) at the liquid-liquid interface. Qualitatively speaking, the velocity (V) at the liquid-gas interface exhibits the same trends as that at the liquid-liquid interface. This follows from Equation (27*a*), which indicates that V_c differs from $\hat{V}_c$ only by the factor $(1/[\cosh \pi D_1 + (\pi\epsilon/\eta y_0) \sinh \pi D_1])$.

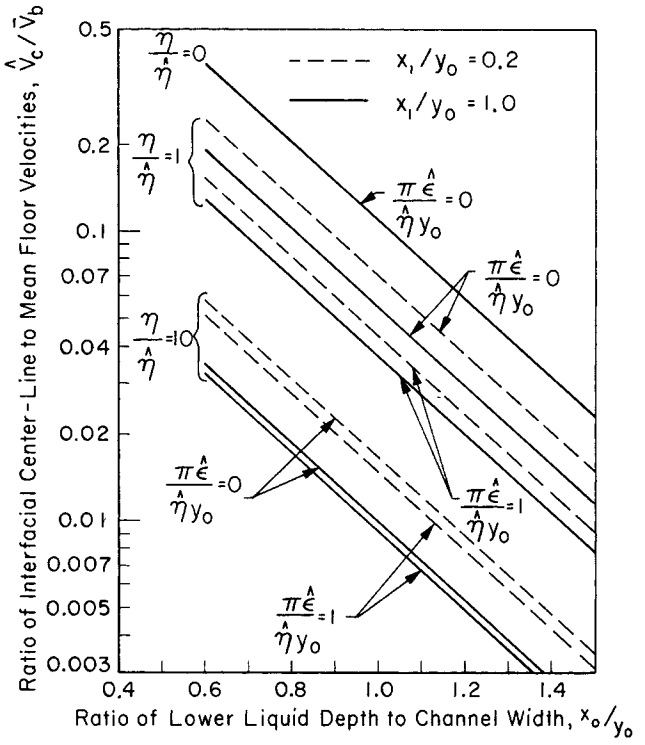

Fig. 5. Theoretical interfacial center-line velocities for $\pi\epsilon/\eta y_0 = 0$.

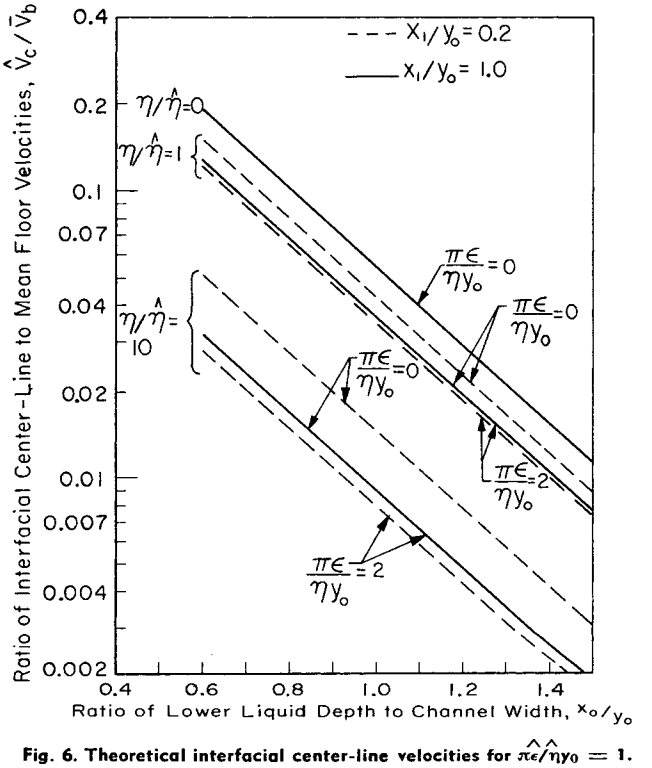

Fig. 6. Theoretical interfacial center-line velocities for $\hat{\pi\epsilon}/\hat{\eta y_0} = 1$.

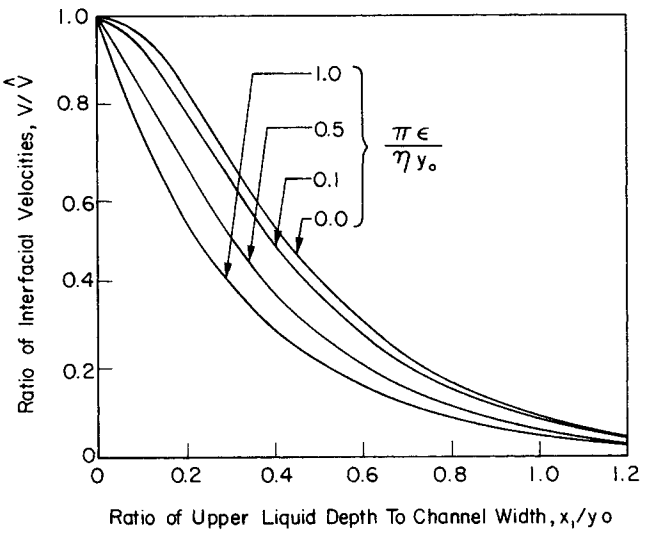

Fig. 7. Relationship between velocities at liquid-liquid and liquid-gas interfaces in liquid-liquid-gas systems.

Since $V = V_c \sin(\pi y/y_0)$ and $\hat{V} = \hat{V}_c \sin(\pi y/y_0)$, as may be seen from Equations (26) and (35), respectively, V and $\hat{V}$ are also related by the above factor. Furthermore, this factor decreases with increasing dimensionless depth of the upper liquid ($D_1 = x_1/y_0$) and increasing dimensionless interfacial viscosity ($\pi\epsilon/\eta y_0$) at the liquid-gas interface. Earlier we have pointed out that $\hat{V}$ displays similar dependence on (x_1/y_0) and ($\pi\epsilon/\eta y_0$) and consequently the effects of these parameters and $\hat{V}$ on V are cumulative. The quantitative dependence of the velocity ratio $V/\hat{V}$ on (x_1/y_0) and ($\pi\epsilon/\eta y_0$) is shown in Figure 7. It is to be observed that this velocity ratio is independent of the dimensionless depth (D) of the lower liquid, the bulk viscosity ratio ($\eta/\hat{\eta}$), and the dimensionless interfacial viscosity ($\hat{\pi\epsilon}/\hat{\eta y_0}$) at the liquid-liquid interface. These parameters affect V and $\hat{V}$ identically.

Experimental Results

Experimental measurements of midchannel velocities were made at various liquid-liquid and liquid-gas interfaces for uncontaminated systems. None of the systems investigated exhibited surface aging or time-dependent interfacial flow. The physical properties are listed in Table 1.

The pure xylene-water interface was studied to assess the effect of the depth of the upper liquid on the interfacial velocity. Two different heights of xylene were used: 0.46 and 0.22 cm. The ratio of the midchannel velocity to the average velocity at the base of the dish, $\hat{V}_c/\bar{V}_b$, is plotted against the ratio (x_0/y_0) of the depth of the lower liquid to the channel width on a semilog plot. In Figure 8 the experimental data for three different depths of the

TABLE 1. PHYSICAL PROPERTIES OF LIQUIDS

Temperature = 27° to 29°C.

Liquid	Density, g./cu.cm.	Bulk viscosity, centipoise
Deionized water	0.9971	0.95
Xylene	0.8563	0.77
Cetane	0.7680	3.06

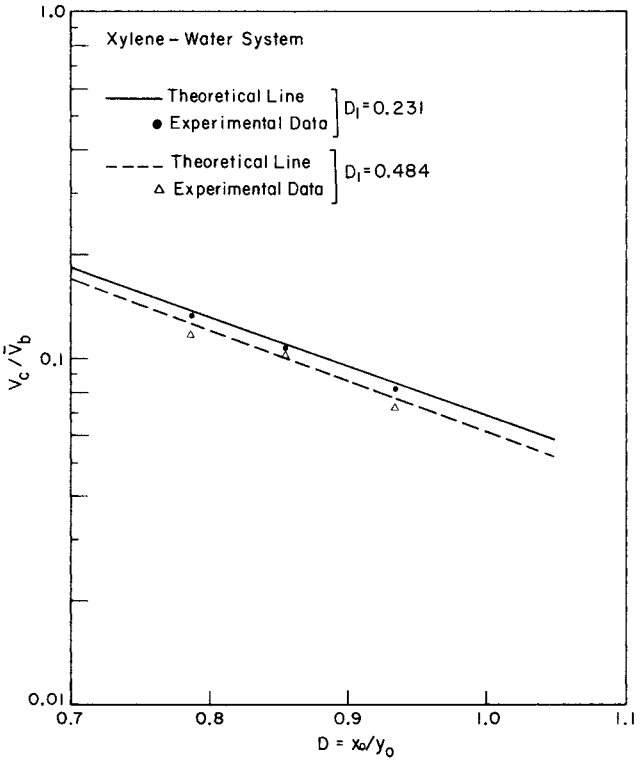

Fig. 8. Effect of upper liquid depth on center-line velocity at the xylene-water interface.

lower liquid are plotted and compared with the theoretical predictions on the basis of Equation (28), incorporating the correction factor (E) due to curved interfaces as given in Table 2.

The experimental midchannel interfacial velocity data for the xylene-water system agree with the theory to within 4%. The deviation may be attributed to experimental error, changes in room humidity, and impurities in the reagent grade xylene and deionized water. Furthermore, we can see clearly from Equation (28) that increasing the ratio (D_1) of the depth of the upper liquid to the width of the channel, and thus decreasing $\tanh \pi D_1$, will lead to increased interfacial velocity for fixed D, $\hat{\eta}$, and η. The experimental results confirm this.

Next the cetane-water interface was investigated. Equation (28) predicts that a plot of the interfacial midchannel velocity ($\hat{V}_c^*$) versus the average velocity of the rotating dish ($\bar{V}_b$), that is, W_c versus W_0 for an uncontaminated system, will be a straight line for fixed D, D_1, $\hat{\eta}$, and η. Figure 9, which displays the theoretical values of W_c for flat as well as curved interfaces, represents such a plot for the cetane-water interface. Use has been made of the correction factor due to curved interfaces as tabulated in Table 2. The mean deviation of data from the theory for curved interfaces is within 2.5%.

Table 2. Correction Factor (E) Due to Curved Interfaces

System	E
Xylene-air	0.9255
Cetane-air	0.9228
Water-xylene*	0.9370
Water-xylene†	0.9782
Water-cetane†	0.9787

* $D_1 = 0.231$.
† $D_1 = 0.484$.

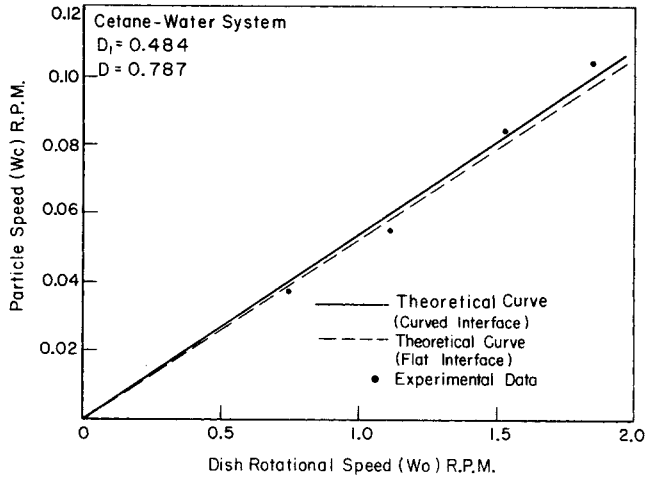

Fig. 9. Particle speed as a function of dish rotational speed for cetane-water interface.

Figure 10 displays W_c versus W_0 for the xylene-air interface (over water). Again the data are in excellent agreement with the theory for curved interfaces. The maximum deviation was found to be 3%.

In addition to the xylene-water and cetane-water systems, the xylene-air and cetane-air systems were also studied independently. Table 3 compares the theoretical and experimental values of the ratio of midchannel interfacial velocities to dish rotational speed for these systems. The agreement between the two is generally satisfactory. The deviation from theory may be attributed to the impurities in the systems. For the experimental work commercial solvents were used, whereas the theory predicts the values for ultrapure systems. The relatively high deviation for the xylene-air system is suspected to be due to secondary flow occurring even at the low dish rotational speeds used.

The results of the theoretical analysis discussed earlier clearly demonstrate the coupling of the interfacial and bulk fluid flows. Theory predicts lower interfacial velocity for higher internal bulk viscosity ratio $\eta/\hat{\eta}$. Experimental data confirm this (see Table 3).

Some work has been done in our laboratory on the effects of surfactants such as stearic acid and ocenol (oleyl

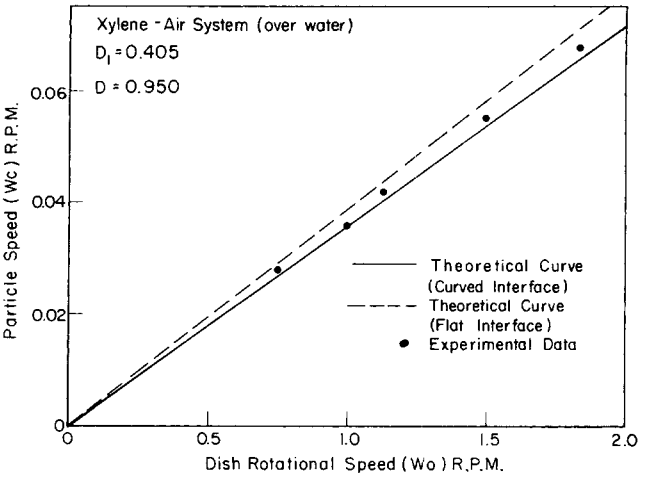

Fig. 10. Particle speed as a function of dish rotational speed for xylene-air interface (over water).

TABLE 3. TYPICAL INTERFACIAL FLOW DATA

System	$\eta/\hat{\eta}$	σ, dynes/cm.	W_c/W_o Theoretical	W_c/W_o Experimental	% Deviation from theory
Xylene-air*	0	27.7	0.1247	0.1253	−10.0%
Cetane-air*	0	25.4	0.1250	0.1125	+0.5%
Water-xylene†	0.81	37.2	0.1220	0.1173	−3.8%
Water-cetane†	3.22	45.1	0.0535	0.0525	−1.8%
Xylene-air (over water)‡	0	27.7	0.0360	0.0370	+2.7%

* $D = 0.935$.
† $D = 0.787$, $D_1 = 0.484$.
‡ $D = 0.950$, $D_1 = 0.405$.

alcohol) on the shear flow at xylene-water interfaces. The interfacial flow data have been interpreted in accordance with the model presented here (*30, 32*).

CONCLUSIONS

The results obtained here lead to the following conclusions:

The present theoretical analysis predicts that increasing interfacial shear viscosity at either the liquid-liquid or the liquid-gas interface results in lower velocity at the liquid-liquid interface in three-phase systems. This effect is more pronounced at low values of upper liquid depths. For large depths of the upper liquid the velocity at the liquid-liquid interface is independent of the interfacial viscosity at the liquid-gas interface.

The theory predicts that for $\pi\epsilon/\eta y_0 < 1$, increasing the upper fluid depth results in decreased velocities and for $\pi\epsilon/\eta y_0 > 1$, increasing the upper fluid depth results in increased velocities. For $\pi\epsilon/\eta y_0 = 1$, the upper fluid depth has no effect on the velocity at the liquid-liquid interfaces (see Figure 6).

The present analysis takes full account of the coupling of interfacial and bulk fluid flows. The theory predicts that increasing the internal bulk viscosity ratio $\eta/\hat{\eta}$ serves to lower the interfacial velocity. The experimental data support this conclusion.

For the uncontaminated water-xylene interface, the values of the midchannel velocity agree within 4% of the present theory; for the cetane-water interface the agreement is within 2.5%.

Finally, it is concluded that the present results permit interpretation of the interfacial shear viscosity at liquid-liquid and liquid-gas interfaces with an improved viscous traction surface viscometer.

ACKNOWLEDGMENT

This study was conducted with the financial assistance of the National Science Foundation under Grant GK-10756.

NOTATION

a_n, b_n, c_n, d_n = constants in Equation (12)
$\hat{a}_n$, $\hat{b}_n$, $\hat{c}_n$, $\hat{d}_n$ = constants in Equation (11)
D = depth of lower liquid/channel width, dimensionless
D_1 = depth of upper liquid/channel width, dimensionless
E = correction factor for curved interfaces
E_n = defined in Equation (22)
n = index in the series expressions for the velocity profile
r_i = radius of the inner cylinder, cm.
r_o = radius of the outer cylinder, cm.
S = interfacial area, sq.cm.
V = fluid velocity in the z direction, cm./sec.
$\overline{V}_b$ = center-line velocity at the channel floor, cm./sec.
V_c = interfacial center-line velocity for systems of finite surface or interfacial viscosity, uncorrected for curvature of the interfaces, cm./sec.
V_c^* = interfacial center-line velocity for systems of negligible surface or interfacial viscosity, uncorrected for curvature of the interfaces, cm./sec.
V_c^{**} = interfacial center-line velocity for systems of negligible surface or interfacial viscosity, corrected for curvature of the interfaces, cm./sec.
W_0 = dish rotational speed, rev./min.
W_c = rotational speed of particle at interfacial center line, rev./min.
x_0 = depth of lower liquid, cm.
x_1 = depth of upper liquid, cm.
y_0 = channel width, cm.
z_0 = depth of lower liquid, cm.
z_1 = depth of upper liquid, cm.

Greek Letters

ϵ = surface or interfacial viscosity, surface poise
η = bulk viscosity of the fluid, poise
λ_n = constant in Equations (11) and (12)
ω_0 = angular velocity of floor, radians/sec.

Subscript

c = interfacial center line

Superscripts

$\wedge$ = lower liquid or interface
$*$ = system of negligible surface or interfacial viscosity

LITERATURE CITED

1. Blakey, B. C., and A. S. C. Lawrence, *Discussions Faraday Soc.*, 18, 268 (1954).
2. Burton, R. A., and R. J. Mannheimer, *Advan. Chem. Ser.*, 63, 315 (1967).
3. Criddle, D. W., and A. L. Meader, *J. Appl. Phys.*, 26, 838 (1955).

4. Cumper, C. W. N., and A. E. Alexander, *Trans. Faraday Soc.*, **46**, 235 (1950).
5. Davies, J. T., and G. R. A. Mayers, *ibid.*, **56**, 690 (1960).
6. Davies, J. T., and E. K. Rideal, "Interfacial Phenomena," 2nd edit., Academic Press, New York (1963).
7. Elenkov, D., *Teoret. Osnovy Khim. Tekhnol.*, **1**, (2), 158 (1967).
8. Gaines, G. L., "Insoluble Monolayers at Liquid-Gas Interfaces," Interscience, New York (1966).
9. Gibbs, J. W., *Trans. Conn. Acad.*, **3**, 343 (1878); "Collected Works," Vol. 1, Longmans-Green, New York (1931).
10. Gupta, L., M.S. thesis, Illinois Inst. Technol., Chicago (1970).
11. Hsu, G. C., and R. C. Kintner, *J. Chem. Eng. Data*, **14**, (1), 67 (1969).
12. Huang, W. S., and R. C. Kintner, *AIChE J.*, **15**, 735 (1969).
13. Israel, A. B., M.S. thesis, Illinois Inst. Technol., Chicago (1968).
14. Joly, M., *J. Colloid Sci.*, **11**, 519 (1956).
15. ———, in "Recent Progress in Surface Science," J. F. Dannielli, K. G. A. Pankhurst, and A. C. Riddiford, Eds., Vol. 1, Academic Press, New York (1964).
16. Kanner, B., and J. E. Glass, *Ind. Eng. Chem.*, **61**, (5), 31 (1969).
17. Karam, H. J., J. C. Bellinger, and R. Z. Balwinski, paper presented at AIChE 60th Ann. Meeting, New York (Nov. 1967).
18. Kintner, R. C., "Advances in Chemical Engineering," T. B. Drew, et al., Eds., Vol. 4, Academic Press, New York (1963).
19. Knapik, H. P. G., M.S. thesis, Illinois Inst. Technol., Chicago (1969).
20. Landau, L. D., and E. M. Lifshitz, "Fluid Mechanics," Permagon Press, London (1959).
21. Levich, V. C., "Physicochemical Hydrodynamics," Prentice-Hall, Englewood Cliffs, N. J. (1962).
22. Mannheimer, R. J., *AIChE J.*, **15**, (1), 88 (1969).
23. ———, and R. S. Schechter, *J. Colloid Interface Sci.*, **32** (2), 195 (1970).
24. Osborne, M. F. M., *Kolloid-Z. Polymere*, **2**, 150 (1967).
25. Pintar, A. J., Ph.D. thesis, Illinois Inst. Technol., Chicago (1968).
26. ———, A. B. Israel, and D. T. Wasan, paper presented at ACS meeting, Chicago (Sept. 13-18, 1970).
27. Shah, S. T., D. T. Wasan, and R. C. Kintner, submitted to *Chem. Eng. Sci.*
28. Sherman, P., *J. Colloid. Sci.*, **8**, 35 (1953).
29. Sternling, C. V., and L. E. Scriven, *AIChE J.*, **5**, 514 (1959).
30. Vora, M. K., M.S. thesis, Illinois Inst. Technol., Chicago (1970).
31. Wasan, D. T., A. J. Pintar, and M. K. Vora, paper presented at AIChE, Washington, D.C. meeting (Nov. 16-20, 1969).
32. Wasan, D. T., L. Gupta, M. K. Vora, and S. T. Shah, manuscript in preparation.

Manuscript received June 7, 1970; revision received September 12, 1970; paper accepted September 21, 1970. Paper presented at AIChE Chicago meeting.

Models for Vapor-Phase and Liquid-Phase Mass Transfer on Distillation Trays

G. A. HUGHMARK

Ethyl Corporation, Baton Rouge, Louisiana 70821

Three mass transfer models are developed for the vapor phase. The first model assumes a rigid interface between the liquid and vapor and yields the Schmidt number as the correlating variable. The other two models represent a free interface with the penetration theory as the mechanism for one model and eddy diffusion as the mechanism for the other model. Both free interface models correlate experimental data within the error of the data. A liquid-phase mass transfer model is developed for a free interface and the penetration theory as the mass transfer mechanism. Design equations are developed from this analysis.

The AIChE Bubble-Tray Design Manual (*1*) proposes models for mass transfer in the vapor and liquid phases of bubble-cap trays. The models are based upon experimental data obtained as part of this research program. Correlation equations for the vapor and liquid phases are

$$N_G = (0.776 + 0.116\,W - 0.29\,F + 0.0217\,L)/(N_{Sc})^{0.5} \quad (1)$$

$$N_L = 6180\,(0.26\,F + 0.15)\,t_L(D_L)^{0.5} \quad (2)$$

Application of the AIChE design method has indicated that liquid-phase-controlled binary systems operating at low liquid rates have much lower efficiencies than are predicted by the design method (2). Hughmark (3) analyzed the AIChE data and proposed a single surface renewal model for the vapor phase with the penetration theory. A more recent analysis (*4*) of University of Michigan humidifica-